12 Correlated Electron Dynamics and Nonequilibrium Dynamical Mean-Field Theory

Marcus Kollar
Center for Electronic Correlations and Magnetism
University of Augsburg

Contents

E. Pavarini, E. Koch, D. Vollhardt, and A. Lichtenstein
DMFT at 25: Infinite Dimensions
Modeling and Simulation Vol. 4
Forschungszentrum Jülich, 2014, ISBN 978-3-89336-953-9
http://www.cond-mat.de/events/correl14

1 Introduction

In Chapters 1 and 3, it was discussed how the limit of infinite lattice dimension $d \to \infty$ [1] leads to drastic simplifications for many-body theory, which describes interacting electrons in their ground state or in thermodynamic equilibrium. In particular, Hubbard-type models in the thermodynamic limit are mapped exactly onto effective single-site problems with a local self-energy, which in turn may be represented as self-consistent single-impurity Anderson models that can be solved numerically. For systems in dimension $d = 1$, 2, 3 this approach corresponds to a mean-field approximation, i.e. to dynamical mean-field theory (DMFT) [2], which can be further improved by including corrections for finite dimensions, see e.g., Chapters 9 and 10.
DMFT can also be applied to nonequilibrium problems, i.e., the single-band Hubbard model with time-dependent hopping amplitudes and interaction parameter,

$$H_{\text{Hubbard}}(t) = \sum_{ij\sigma} t_{ij}(t)\, c^\dagger_{i\sigma} c_{j\sigma} + U(t) \sum_i (n_{i\uparrow} - \tfrac{1}{2})(n_{i\downarrow} - \tfrac{1}{2})\,. \tag{1}$$

Due to recent experimental advances, theoretical methods to study such systems are of great interest. Correlated materials can be excited and their relaxation monitored using pump-probe spectroscopy with femtosecond laser pulses [3,4]. In a suitable gauge, the electric field couples to the band energies via the time-dependent vector potential according to the Peierls substitution [5],

$$t_{ij}(t) = t_{ij} \exp\left(-\frac{ie}{\hbar} \int_{\boldsymbol{R}_i}^{\boldsymbol{R}_j} d\boldsymbol{r} \cdot \boldsymbol{A}(\boldsymbol{r}, t) \right). \tag{2}$$

However, after a few hundred femtoseconds the electronic degrees of freedom will typically have relaxed and their coupling to the slower vibrational lattice degrees of freedom will come into play. From a quite different perspective, it is also possible to study the real-time behavior of many-body states using ultracold atomic gases in optical lattices, which can be kept in excellent isolation from the environment and for which kinetic and interaction energies can be controlled very precisely for many hundreds of microseconds [6,7].
In general, many-body theory for nonequilibrium is numerically even more demanding than for equilibrium. For systems in equilibrium, the main task is to evaluate expectation values (such as Green functions) for a grand-canonical density matrix (such as a thermal state for an interacting Hamiltonian or possibly its ground state). In nonequilibrium, additionally, the time evolution under a time-dependent Hamiltonian must be taken into account. However, using nonequilibrium Green functions according to the Keldysh formalism, the limit of infinite lattice dimensions provides similar benefits as in the equilibrium case, i.e., the problem is again reduced to a single site by integrating out the rest of the lattice, although the remaining nonequilibrium impurity problem is more complicated than in equilibrium. The nonequilibrium DMFT approach was first developed and applied for the Falicov-Kimball model [8–15] (following an earlier incomplete attempt in Ref. [16]). Since then, many more applications and extensions have appeared, including for time-resolved spectroscopy [17–19], abrupt and slow

changes in parameters [20–26], response to DC and AC fields and pulses [27–43], antiferromagnetic phases [44–47], coupling to phonons [48, 49], inhomogeneous systems [50], extensions for lower dimensions [51–53], and dynamics of lattice bosons [54]. A recent review of the nonequilibrium DMFT and its applications can be found in Ref. [55].
Below, the main ingredients for nonequilibrium DMFT are discussed. First, nonequilibrium Green functions are defined according to the Keldysh formalism (Sec. 2). Then, the mapping of a Hubbard model to a single-site problem with a dynamic bath is discussed (Sec. 3). Finally, some aspects of the single-band Hubbard model in nonequilibrium (Sec. 4) are reviewed. We follow mostly the setup and notation of Refs. [55] and [26].

2 Nonequilibrium Green functions

2.1 Time contour

We consider the time evolution of a quantum many-body system with density matrix $\rho(t)$ that starts at time $t = 0$ from thermal equilibrium, i.e., from a grand-canonical Gibbs state of the Hamiltonian $H(0)$,

$$\rho(0) = \frac{1}{Z} e^{-\beta \mathcal{H}(0)}, \tag{3}$$

i.e., the classical superposition of all eigenstates of the Hamiltonian depending on their Boltzmann weights. Here $\beta = 1/(k_{\mathrm{B}} T)$ is the inverse temperature, $k_{\mathrm{B}} = 1$, $\mathcal{H}(t) = H(t) - \mu N(t)$, with μ the chemical potential, $N(t)$ the particle number operator, and $Z = \mathrm{Tr}\, e^{-\beta \mathcal{H}(0)}$ the equilibrium partition function. At time $t = 0$ the Hamiltonian changes, either continuously or abruptly, e.g., by switching on an electric field. The time-dependent Schrödinger equation then determines the evolution of the wave function, which is continuous in t. For a density matrix, this yields the von Neumann equation ($\hbar = 1$) and its formal solution,

$$i \frac{d}{dt} \rho(t) = [\mathcal{H}(t), \rho(t)]\,, \qquad\qquad \rho(t) = U(t,0)\, \rho(0)\, U(0,t)\,. \tag{4}$$

Our goal is to obtain the time-dependent expectation value of a (time-independent) Schrödinger operator A,

$$\langle A \rangle_t = \mathrm{Tr}[\rho(t) A]\,. \tag{5}$$

The propagator obeys $\frac{d}{dt} U(t,t') = -i \mathcal{H}(t) U(t,t')$, hence it is unitary, $U(t,t') U(t,t')^\dagger = U(t,t') U(t',t) = 1$, and fulfills $U(t,t') U(t',t'') = U(t,t'')$. Because $\mathcal{H}(t)$ and $\mathcal{H}(t')$ do not in general commute at different times, the formal solution of the differential equation for $U(t,t')$ is

$$U(t,t') = \begin{cases} \mathrm{T} \exp\left(-i \displaystyle\int_{t'}^{t} d\bar{t}\, \mathcal{H}(\bar{t}) \right) & \text{for } t > t'\,, \\ \bar{\mathrm{T}} \exp\left(-i \displaystyle\int_{t'}^{t} d\bar{t}\, \mathcal{H}(\bar{t}) \right) & \text{for } t < t'\,, \end{cases} \tag{6}$$

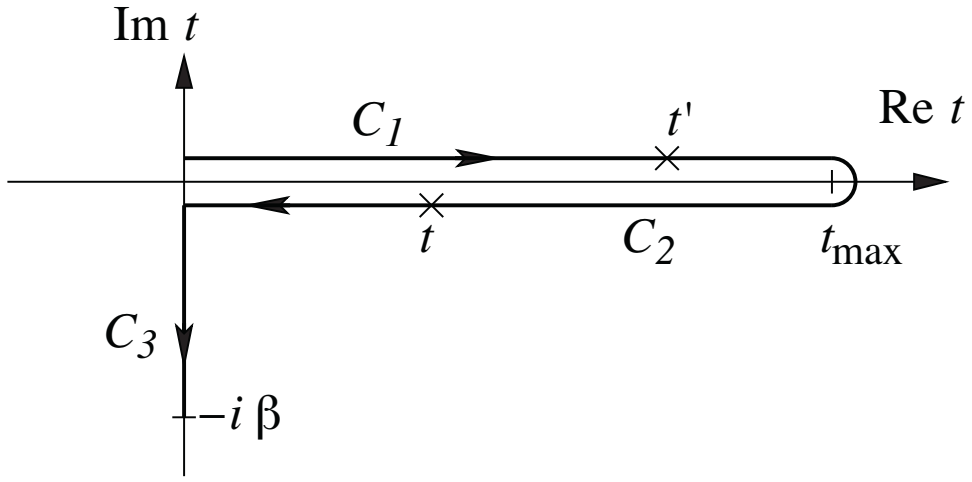

Fig. 1: *The integration along the L-shaped integration contour C runs along C_1 from 0 to t_{max} on the real axis, goes back along C_2, and proceeds along C_3 to $-i\beta$. In the figure, the times $t \in C_2$ and $t' \in C_1$ are located such that $t >_C t'$, i.e., t is later than t' in the sense of contour ordering.*

where T and $\bar{\mathrm{T}}$ denote time-ordering and anti-time-ordering operators, respectively; i.e., T reorders the operators $\mathcal{H}(\bar{t})$ that occur in the expansion of the exponential such that the time arguments $\bar{t}$ increase from right to left (and from left to right for $\bar{\mathrm{T}}$). The density matrix $\rho(t)$ in the time-dependent expectation value (5) then involves one exponential with a forward integration along the time axis due to $U(t,t')$, one with a backwards integration due to $U(t',t)$, and in between sits $\exp(-\beta\mathcal{H}(0))$ representing the initial state, the exponent of which can be rewritten as an integral with respect to t from 0 to $-i\beta$ of $\mathcal{H}(0)$. The time ordering of operators $\mathcal{H}(\bar{t})$ in (5) thus involves three parts, C_1: $0 \ldots t_{\mathrm{max}}$, C_2: $t_{\mathrm{max}} \ldots 0$, and C_3: $0 \ldots -i\beta$ (where t_{max} is the maximal time of interest)

$$\begin{aligned} \langle A \rangle_t &= \frac{1}{Z} \mathrm{Tr}[U(-i\beta,0)U(0,t)\, A\, U(t,0)] \\ &= \frac{\mathrm{Tr}\, \mathrm{T}_C\, A(t)\, \exp[-i\int_C d\bar{t}\, \mathcal{H}(\bar{t})]}{\mathrm{Tr}\, \mathrm{T}_C\, \exp[-i\int_C d\bar{t}\, \mathcal{H}(\bar{t})]} \,. \end{aligned} \tag{7}$$

The integrals in the last expression are now along an L-shaped contour C that runs along C_1, C_2, and then C_3; T_C is the contour-ordering operator that arranges operators on C in the direction of the arrows in Fig. 1. The time argument t that has been attached to $A(t)$ merely indicates the time at which the (Schrödinger) operator A must be inserted in the contour time ordering. In the denominator of (7), no operator is inserted and hence the contributions from C_1 and C_2 cancel, yielding the partition function. The time parametrization along a contour allows to carry over many techniques from equilibrium many-body theory [56] (such as Feynman diagrams etc.), although it does not mean that integrations are actually performed in the complex plane. Rather, the contributions of the contour parts C_1, C_2, C_3 are evaluated separately. In particular, the following definitions for contour integrals, contour convolutions, time derivative, contour

theta and delta functions are useful:

$$g(t \in C) = \begin{cases} g^+(t) & \text{if } t \in [0, t_{\max}] \text{ on } C_1, \\ g^-(t) & \text{if } t \in [0, t_{\max}] \text{ on } C_2, \\ g^|(-i\tau) & \text{if } t = -i\tau \text{ on } C_3,\ \tau \in [0, \beta], \end{cases} \tag{8}$$

$$\int_C dt\, g(t) = \int_0^{t_{\max}} dt\, g^+(t) - \int_0^{t_{\max}} dt\, g^-(t) - i \int_0^{\beta} d\tau\, g^|(-i\tau)\,, \tag{9}$$

$$[a * b](t, t') = \int_C d\bar{t}\, a(t, \bar{t}) b(\bar{t}, t')\,, \tag{10}$$

$$\partial_t g(t) = \begin{cases} \partial_t g(t^\pm) & t \in C_{1,2} \\ i\partial_\tau g(-i\tau) & t = -i\tau \in C_3 \end{cases}, \tag{11}$$

$$\theta_C(t, t') = \begin{cases} 1 & \text{for } t >_C t'\,, \\ 0 & \text{otherwise,} \end{cases} \tag{12}$$

$$\delta_C(t, t') = \partial_t \theta_C(t, t')\,, \tag{13}$$

$$\int_C d\bar{t}\, \delta_C(t, \bar{t}) g(\bar{t}) = g(t)\,. \tag{14}$$

Here $t >_C t'$ means that t appears later on the contour (as shown in Fig. 1).
The representation of time-dependent expectation values (7), in particular for nonequilibrium Green functions, is called the Keldysh formalism and is based on Refs. [57–59]. Modern introductions to the subject are can be found, e.g., in Refs. [60–62], of which in particular [62] is very detailed, pedagogical, and complete. Note that, depending on the physical situation, other time contours are used in the literature. In particular, the so-called Keldysh contour that extends C_1 and C_2 to $-\infty$ without C_3 is useful to describe transport and nonequilibrium steady states with currents. However, for lattice models like (1) without reservoirs, the L-shaped contour is best suited, as it requires no further assumptions on the form of the nonequilibrium state, switching-on of interactions, etc. Further discussions of various contour shapes can be found, e.g., in Refs. [61–63].

2.2 Contour Green functions

The study of single-particle Green functions is a standard method to characterize the spectrum and state in many-particle systems. For later use the action S is defined for a given Hamiltonian as

$$S = -i \int_C dt\, \mathcal{H}(t)\,, \tag{15}$$

so that $\langle A \rangle_t$ is now written as $\langle A(t) \rangle_S = \mathrm{Tr}[\mathrm{T}_C \exp(S) A(t)]/Z_S$ with $Z_S = \mathrm{Tr}[\mathrm{T}_C \exp(S)]$. If there is no ambiguity we will omit the subscript S. The definition of the time-ordering operator

is changed to

$$\mathrm{T}_C A(t)B(t') = \begin{cases} AB & \text{if } t >_C t', \\ \pm BA & \text{if } t <_C t', \end{cases} \tag{16}$$

where the negative sign is used only if both A and B contain an odd number of fermionic annihilation or creation operators. Furthermore, if t and t' are equal and on the same branch of the contour, T_C performs a normal ordering by convention, moving all creators to the left.
Single-particle contour Green functions for fermions are then defined as contour-ordered expectation values in analogy to the equilibrium case,

$$G(t,t') = -i\langle c(t)c^\dagger(t')\rangle = -\frac{i}{Z}\,\mathrm{Tr}\left[\mathrm{T}_C\left\{\exp(S)c\,(t)c^\dagger(t')\right\}\right], \tag{17}$$

where the basis state indices (e.g., site, spin, and orbital indices) have been omitted on the fermionic creation and annihilation operators for now, so all Green function should be regarded as matrices in these indices. The time arguments t and t' can each lie on one of the three parts of the contour so that G has nine entries with different physical meanings. A subscript $a, b = 1, 2, 3$ on $G_{ab}(t,t')$ then expresses whether a time argument is on the upper (1), lower (2), or imaginary (3) part of the contour C. There is some redundancy because one can shift the operator with the largest real-time argument between C_1 and C_2 because the time evolution along these paths cancels on its right. It follows that

$$G_{11}(t,t') = G_{12}(t,t') \quad \text{for } t \le t', \tag{18a}$$
$$G_{11}(t,t') = G_{21}(t,t') \quad \text{for } t > t', \tag{18b}$$
$$G_{22}(t,t') = G_{21}(t,t') \quad \text{for } t < t', \tag{18c}$$
$$G_{22}(t,t') = G_{12}(t,t') \quad \text{for } t \ge t', \tag{18d}$$
$$G_{13}(t,\tau') = G_{23}(t,\tau'), \tag{18e}$$
$$G_{31}(\tau,t') = G_{32}(\tau,t'). \tag{18f}$$

It is then customary to define the following independent components: retarded (G^R), advanced (G^A), Keldysh (G^K), left-mixing ($G^\urcorner$), right-mixing ($G^\ulcorner$), and Matsubara (G^M) Green function. For t and t' from C_1 or C_2, τ from C_3, and T_τ the imaginary-time ordering operator, they are given by

$$G^R(t,t') = \tfrac{1}{2}(G_{11} - G_{12} + G_{21} - G_{22}) = -i\theta(t-t')\langle\{c(t), c^\dagger(t')\}\rangle, \tag{19a}$$
$$G^A(t,t') = \tfrac{1}{2}(G_{11} + G_{12} - G_{21} - G_{22}) = \;\; i\theta(t'-t)\langle\{c(t), c^\dagger(t')\}\rangle, \tag{19b}$$
$$G^K(t,t') = \tfrac{1}{2}(G_{11} + G_{12} + G_{21} + G_{22}) = \;\; -i\langle[c(t), c^\dagger(t')]\rangle, \tag{19c}$$
$$G^\urcorner(t,\tau') = \tfrac{1}{2}(G_{13} + G_{23}) = \;\; i\langle c^\dagger(\tau')c(t)\rangle, \tag{19d}$$
$$G^\ulcorner(\tau,t') = \tfrac{1}{2}(G_{31} + G_{32}) = -i\langle c(\tau)c^\dagger(t')\rangle, \tag{19e}$$
$$G^M(\tau,\tau') = -iG_{33} = \;\; -\langle \mathrm{T}_\tau\, c(\tau)c^\dagger(\tau')\rangle. \tag{19f}$$

Furthermore, the so-called lesser and greater Green functions are defined as

$$G^<(t,t') = G_{12} = i\langle c^\dagger(t')c(t)\rangle\,, \qquad G^>(t,t') = G_{21} = -i\langle c(t)c^\dagger(t')\rangle\,. \tag{20}$$

They fulfill $G^< = \frac{1}{2}(G^K - G^R + G^A)$ and $G^> = \frac{1}{2}(G^K + G^R - G^A)$. Hermitian conjugation entails the relations

$$G^{<,>,K}(t,t')^* = -G^{<,>,K}(t',t)\,, \tag{21a}$$

$$G^R(t,t')^* = G^A(t',t)\,, \tag{21b}$$

$$G^{\urcorner}(t,\tau)^* = G^{\ulcorner}(\beta-\tau,t)\,. \tag{21c}$$

The Matsubara Green function is translationally invariant, as $\mathcal{H}$ does not depend on τ, i.e., $G^M(\tau,\tau') = G^M(\tau-\tau')$. It is also real and antiperiodic, $G^M(\tau) = -G^M(\tau+\beta)$, so it can be Fourier transformed to Matsubara frequencies as in equilibrium. Finally, the following boundary conditions hold because the trace is cyclic,

$$G(0^+,t) = -G(-i\beta,t)\,, \qquad G(t,0^+) = -G(t,-i\beta)\,. \tag{22}$$

Here and throughout, $G(t,t')$ (without superscript denoting a component) is a contour Green function for which the time arguments can be on any one of C_1, C_2, C_3. By contrast, a Green function with superscript contains (real or imaginary) time arguments for which the contour part need not be specified. A convolution of contour functions $f * g$ involves contributions of several components. The procedures that separate the components of $f * g$ and express them in terms of the components of f and g are called Langreth rules [64]. They are discussed in detail, e.g., in Ref. [62].

2.3 Equilibrium case

For a time-independent Hamiltonian the formalism reduces of course to that for the equilibrium case [56], and only dependencies on time differences remain. In particular, the single-particle spectral function that characterizes the excitation spectrum is given in terms of Fourier transforms as

$$A(\omega) = -\frac{1}{\pi}\,\mathrm{Im}\,G^R(\omega) = \frac{1}{\pi}\,\mathrm{Im}\,G^A(\omega)\,. \tag{23}$$

In equilibrium, all components of G can be recovered from it,

$$G(t,t') = -i\int d\omega\, e^{i\omega(t'-t)}\,A(\omega)\,[\theta_C(t,t') - f(\omega)], \tag{24}$$

where $f(\omega) = 1/(e^{\beta\omega}+1)$ is the Fermi function.
In nonequilibrium, one can introduce average and relative times, $t_{\rm av} = (t+t')/2$, $t_{\rm rel} = t - t'$, in terms of which a partial Fourier transformation leads to the definition

$$A(\omega, t_{\rm av}) = -\frac{1}{\pi}\mathrm{Im}\int dt_{\rm rel}\, e^{i\omega t_{\rm rel}}\,G^R(t,t')\,, \tag{25}$$

which satisfies the sum rule $\int d\omega\, A(\omega, t_{\rm av}) = 1$.

2.4 Noninteracting case

Consider now the simplest case of noninteracting fermions with a single time-dependent energy band, $\mathcal{H}_0(t) = \sum_{\boldsymbol{k}}[\varepsilon_{\boldsymbol{k}}(t) - \mu]\, c^\dagger_{\boldsymbol{k}} c_{\boldsymbol{k}}$. The time derivative of the corresponding noninteracting contour Green function $G_{0,\boldsymbol{k}}(t,t') = -i\langle \mathrm{T}_C c_{\boldsymbol{k}}(t) c^\dagger_{\boldsymbol{k}}(t')\rangle$ yields the equations of motion

$$\big[i\partial_t + \mu - \varepsilon_{\boldsymbol{k}}(t)\big] G_{0,\boldsymbol{k}}(t,t') = \delta_C(t,t'), \tag{26a}$$

$$G_{0,\boldsymbol{k}}(t,t')\big[-i\overleftarrow{\partial}_{t'} + \mu - \varepsilon_{\boldsymbol{k}}(t')\big] = \delta_C(t,t'). \tag{26b}$$

Here we let the derivative $\overleftarrow{\partial}_{t'}$ act to the left, i.e., $f(t)\overleftarrow{\partial}_t = \partial_t f(t)$, which makes the equations more symmetric. The inverse of $G_{0,\boldsymbol{k}}$ is then defined as the following differential operator,

$$G^{-1}_{0,\boldsymbol{k}}(t,t') = \big[i\partial_t + \mu - \varepsilon_{\boldsymbol{k}}(t)\big]\delta_C(t,t')\,. \tag{27}$$

The equations of motion thus correspond to the convolutions,

$$G^{-1}_{0,\boldsymbol{k}} * G_{0,\boldsymbol{k}} = G_{0,\boldsymbol{k}} * G^{-1}_{0,\boldsymbol{k}} = \delta_C. \tag{28}$$

Together with (22), either of these gives the unique solution [8],

$$G_{0,\boldsymbol{k}}(t,t') = -i[\theta_C(t,t') - f(\varepsilon_{\boldsymbol{k}}(0) - \mu)] e^{-i\int_{t'}^{t} d\bar{t}\,[\varepsilon_{\boldsymbol{k}}(\bar{t}) - \mu]}. \tag{29}$$

2.5 Self-energy

For an interacting Hamiltonian $\mathcal{H}(t)$, one usually has to resort to approximations to obtain the Green function G, e.g., by using perturbation expansions in terms of Feynman diagrams [62]. The self-energy $\Sigma(t,t')$ is then defined as a contour function (with boundary conditions as in (22)) in terms of one-particle irreducible diagrams, which are the same as those for finite-temperature equilibrium perturbation theory, but with the imaginary-time integrations in the diagram rules being replaced by time-contour integrations. The full Green function is then given in terms of the noninteracting Green function and self-energy insertions (on the contour), $G = G_0 + G_0 * \Sigma * G_0 + G_0 * \Sigma * G_0 * \Sigma * G_0 + \cdots$. The Dyson equation therefore reads

$$G = G_0 + G_0 * \Sigma * G = G_0 + G * \Sigma * G_0\,. \tag{30}$$

After convoluting these equations with G_0^{-1} from either side this becomes

$$[G_0^{-1} - \Sigma] * G = G * [G_0^{-1} - \Sigma] = \delta_C\,. \tag{31}$$

This suggests the definition $G^{-1} = G_0^{-1} - \Sigma$, which is reminiscent of the equilibrium Dyson equation [56]. However, in the present case the equations for G, even if Σ is known, correspond to integral-differential equations along the contour. Their form will be discussed in more detail in the next section.

3 Nonequilibrium DMFT

The hallmark of DMFT, whether in equilibrium or nonequilibrium, is its formulation in terms of a dynamical effective single-site problem in the thermodynamic limit. The numerical solution of this single-site problem then provides the self-energy (and thus Green functions), often in a nonperturbative way. In this section, we show (following Ref. [26]) how the nonequilibrium DMFT equations are obtained in the limit of infinite lattice dimensions by means of the so-called cavity method, which was already employed in the equilibrium case in Ref. [2]. Alternatively, one can base the derivation on the identical diagrammatic skeleton expansions for the self-energies of the single-impurity Anderson model (SIAM) and the Hubbard model in infinite dimensions [9, 55].

3.1 Cavity method

We start from the Hubbard Hamiltonian (1) and, in the spirit of the cavity method, pick out one single site with the purpose of tracing out the remaining lattice. The action is thus split into

$$S = -i \int_C dt\, \mathcal{H}(t) = S_0 + \Delta S + S^{(0)}, \tag{32}$$

with

$$S_0 = -i \int_C dt \left[U(t) \left(n_{0\uparrow}(t) - \tfrac{1}{2}\right) \left(n_{0\downarrow}(t) - \tfrac{1}{2}\right) - \mu \sum_\sigma n_{0\sigma}(t) \right], \tag{33}$$

$$\Delta S = -i \int_C dt \left[\sum_{i\neq 0,\sigma} t^\sigma_{i0}(t)\, c^\dagger_{i\sigma}(t) c_{0\sigma}(t) + \text{H.c.} \right],$$

$$S^{(0)} = -i \int_C dt\, \mathcal{H}^{(0)}(t). \tag{34}$$

Here $\mathcal{H}^{(0)}(t)$ is the Hamiltonian $\mathcal{H}(t)$ with the cavity site 0 removed. The effective single-site action for this site 0 will consist of S_0 for the local Hamiltonian at site 0 and a connection into the effective environment that comes from integrating out $\Delta S + S^{(0)}$. Splitting the trace for the states at site 0 and the other sites, the partition function takes the form

$$\begin{aligned} Z_S &= \mathrm{Tr}_0 \left[\mathrm{T}_C \left\{ \exp(S_0) \mathrm{Tr}_{\text{rest}} \left(\exp(\Delta S + S^{(0)}) \right) \right\} \right] \\ &= Z_{S^{(0)}} \mathrm{Tr}_0 \left[\mathrm{T}_C \left\{ \exp(S_0 + \tilde{S}) \right\} \right], \qquad Z_{S^{(0)}} = \mathrm{Tr}_{\text{rest}} \left(\mathrm{T}_C \left\{ \exp\left(S^{(0)}\right) \right\} \right). \end{aligned} \tag{35a}$$

Here $\tilde{S}$ is the effective action connecting the cavity site and the environment:

$$\exp(\tilde{S}) = \sum_{n=0}^{\infty} \frac{1}{n!} \langle (\Delta S)^n \rangle_{S^{(0)}}, \qquad \langle A(t) \rangle_{S^{(0)}} \equiv \frac{\mathrm{Tr}_{\text{rest}} \left(\mathrm{T}_C \left\{ \exp\left(S^{(0)}\right) A(t) \right\} \right)}{Z_{S^{(0)}}} \tag{36}$$

Note that here ΔS contains operators at site 0 that are not traced over; since they anticommute with those at other sites, the correct sign and time ordering must be kept when tracing over

the latter. From the definition of ΔS, we see that only terms with an equal number of $c^\dagger_{i\sigma}, c_{j\sigma}$ with $i, j \neq 0$ contribute, i.e., only terms with even powers of ΔS. After some combinatorial considerations and reorderings, the result is [26]

$$\exp(\tilde{S}) = \sum_{n=0}^{\infty} \frac{1}{(2n)!} \langle (\Delta S)^{2n} \rangle_{S^{(0)}} = \sum_{n=0}^{\infty} \int_C dt_1 \cdots \int_C dt'_n \sum_{\substack{i_1,\ldots,j_n \\ \sigma_1,\ldots,\sigma'_n}} (-i)^n \times \frac{t_{0i_1}(t_1) \ldots t_{j_n 0}(t'_n)}{n!^2} \, G^{(0)}_{i_1\sigma_1,\ldots,j_n\sigma'_n}(t_1,\ldots,t'_n) \, c^\dagger_{0\sigma_1}(t_1) \ldots c_{0\sigma'_n}(t'_n) \,, \quad (37)$$

with the n-particle contour-ordered Green function for the rest of the lattice (without site 0) defined as

$$G^{(0)}_{i_1\sigma_1,\ldots,j_n\sigma'_n}(t_1,\ldots,t'_n) = (-i)^n \langle c_{i_1\sigma_1}(t_1) \ldots c^\dagger_{j_n\sigma'_n}(t'_n) \rangle_{S^{(0)}} \,. \quad (38)$$

Next, the right-hand side of (37) must be re-exponentiated using connected (with respect to the interaction in $\mathcal{H}^{(0)}(t)$) contour-ordered Green functions $G^{(0),c}$ [26]. The result is

$$\tilde{S} = -i \sum_{n=1}^{\infty} \sum_{\sigma_1 \ldots \sigma'_n} \int_C dt_1 \ldots \int_C dt'_n \, \Lambda_{\sigma_1 \ldots \sigma'_n}(t_1,\ldots,t'_n) \, c^\dagger_{0\sigma_1}(t_1) \ldots c_{0\sigma'_n}(t'_n), \quad (39)$$

where we defined the nth-order hybridization functions

$$\Lambda_{\sigma_1 \ldots \sigma'_n}(t_1,\ldots,t'_n) \equiv \frac{(-i)^{n-1}}{n!^2} \sum_{i_1,\ldots,j_n} t_{0i_1}(t_1) \cdots t_{j_n 0}(t'_n) \, G^{(0),\mathrm{c}}_{i_1\sigma_1,\ldots,j_n\sigma'_n}(t_1,\ldots,t'_n), \quad (40)$$

which involve connected cavity Green functions $G^{(0),\mathrm{c}}$ that are obtained with $S^{(0)}$ only.
The effective action and its partition function, which only involve the degrees of freedom at the cavity site 0, are thus given by

$$S_{\text{eff}} = S_0 + \tilde{S}, \qquad Z_{\text{eff}} = \frac{Z}{Z_{S^{(0)}}} = \mathrm{Tr}_0 \left(\mathrm{T}_C \left\{ \exp(S_{\text{eff}}) \right\} \right). \quad (41)$$

No approximation has been made yet, but of course the higher-order hybridization functions (40) are not easily accessible in general and also couple to correspondingly complicated cavity source terms. In this formulation, the limit of infinite dimensions lets only the hybridization functions with $n = 1$ contribute, leading to a quadratic coupling between cavity and environment, which we now discuss.

3.2 DMFT action for an infinite-dimensional lattice

As in equilibrium [2], the hybridization functions (40) simplify drastically in the limit $d \to \infty$. As a consequence of the quantum scaling [1] $t_{ij} \propto \mathcal{Z}_{ij}^{-\frac{1}{2}}$, where $\mathcal{Z}_{ij}$ is the number of sites j connected to site i by hopping of type t_{ij}, only first-order terms (i.e., one-particle Green functions) contribute to the effective action. These power counting arguments are entirely analogous to

the equilibrium case. For the case of nearest-neighbor hopping on a hypercubic lattice, they proceed as follows.

The contributions to (40) from nth order Green functions contain lattice summations that yield a factor d^{2n}, $2n$ factors of hopping amplitudes $t_{0i} \propto d^{-1/2}$ giving d^{-n}, and a factor from the connected Green functions. The latter connects $2n$ nearest neighbors of 0, with the shortest path between them requiring 2 lattice steps, of which at least $2n-1$ are needed, and in the best case (when all sites are different) this gives a factor $(\sqrt{d})^{2(2n-1)} = d^{2n-1}$. Hence

$$\Lambda_{\sigma_1\ldots\sigma'_n}(t_1,\ldots,t'_n) \propto \underbrace{\sum_{i_1,\ldots,j_n}}_{\propto d^{2n}} \underbrace{t_{0i_1}(t_1)\ldots t_{j_n0}(t'_n)}_{\propto(\sqrt{d})^{-2n}} \underbrace{G^{(0),\mathrm{c}}_{(i_1\sigma_1),\ldots,(j_n\sigma'_n)}(t_1,\ldots,t'_n)}_{\propto(\sqrt{d})^{-2(2n-1)}} \propto \frac{1}{d^{n-1}}\,, \tag{42}$$

so that for $d\to\infty$ only the quadratic term $n=1$ survives. Furthermore, Λ is spin-diagonal as (1) does not contain spin-flip terms. Dropping the index 0 of the cavity site, the DMFT action is therefore

$$\boxed{\begin{aligned} S_{\mathrm{loc}} = -i\int_C dt\Big[U(t)\left(n_\uparrow(t)-\tfrac{1}{2}\right)\left(n_\downarrow(t)-\tfrac{1}{2}\right) - \mu\sum_\sigma n_\sigma(t)\Big] \\ - i\int_C dt_1\int_C dt_2 \sum_\sigma \Lambda_\sigma(t_1,t_2)\, c^\dagger_\sigma(t_1) c_\sigma(t_2). \end{aligned}} \tag{43}$$

It remains to determine the hybridization Λ defined as

$$\Lambda_\sigma(t,t') = \sum_{i,j} t_{0i}(t)\, G^{(0),c}_{ij\sigma}(t,t')\, t_{j0}(t')\,, \tag{44}$$

such that the action indeed describes the original interacting lattice system. This requires linking the Green function $G^{(0),c}_{ij\sigma}$ to local quantities (using the self-energy, which turns out to be local). Physically, the hybridization characterizes the "dynamical mean-field", i.e., the effective host into and out of which the particles on the impurity site can move.

Comparing the nonequilibrium DMFT action (43) with the equilibrium case, we note of course the appearance of time-contour integrals and ordering. Furthermore, the action is not time-translationally invariant because Λ depends explicitly on t and t'. This complicates the task of numerically obtaining G from S for a given Λ.

3.3 Local self-energy

The local nature of the self-energy in infinite dimensions can be obtained from the cavity method itself, as we now describe. It enters into the lattice and impurity Dyson equations, which determine the corresponding lattice and impurity Green functions. In general, the self-energy is also needed to obtain the self-consistency relation for Λ. For brevity, we now drop the spin indices. The hopping $t_{ij}(t)$ is again arbitrary.

We consider the full lattice Green function $G_{ij}(t,t') = -i\langle c_i(t) c^\dagger_j(t')\rangle_S$ on the one hand and the impurity Green function $G(t,t') = G_{00}(t,t')$ on the other. Their inverses are given by $G^{-1}_{\mathrm{lat}}(t,t')$

and $G^{-1}(t,t')$ respectively,

$$\sum_l \int_C dt_1 (G^{-1}_{\text{lat}})_{il}(t,t_1) G_{lj}(t_1,t') = \delta_{ij}\delta_C(t,t')\,, \tag{45a}$$

$$\int_C dt_1 G^{-1}(t,t_1) G(t_1,t') = \delta_C(t,t')\,. \tag{45b}$$

The corresponding impurity and lattice self-energies are then determined by the relations

$$(G^{-1}_{\text{lat}})_{ij}(t,t') = [\delta_{ij}(i\partial_t + \mu) - t_{ij}(t)]\,\delta_C(t,t') - (\Sigma_{\text{lat}})_{ij}(t,t')\,, \tag{46}$$

$$G^{-1}(t,t') = (i\partial_t + \mu)\delta_C(t,t') - \Lambda(t,t') - \Sigma(t,t')\,. \tag{47}$$

Taking functional derivatives of $G_{ij}(t,t')$ with respect to the annihilation and creation operators at site 0 (and hopping matrix elements that connect them) provides the relations [26]

$$G_{ij}(t,t') = G^{(0),c}_{ij}(t,t') + \int_C dt_1 \int_C dt_2 \sum_{lm} G^{(0),c}_{il}(t,t_1)\, t_{l0}(t_1)\, G(t_1,t_2)\, t_{0m}(t_2)\, G^{(0),c}_{mj}(t_2,t'). \tag{48}$$

$$G_{0j}(t,t') = \int_C dt_1 \sum_i G(t,t_1)\, t_{0i}(t_1)\, G^{(0),c}_{ij}(t_1,t')\,, \quad j \neq 0\,. \tag{49}$$

Putting (49) into (48) then gives us

$$G^{(0),c}_{ij}(t,t') = G_{ij}(t,t') - \int_C dt_1 \int_C dt_2\, G_{i0}(t,t_1)\, G^{-1}(t_1,t_2)\, G_{0j}(t_2,t')\,, \tag{50}$$

which we recognize as an analogue of the relation in equilibrium (i.e., Eq. (36) in Ref. [2]): $G^{(0),c}_{ij}(i\omega_n) = G_{ij}(i\omega_n) - G_{i0}(i\omega_n)\, G_{0j}(i\omega_n)/G(i\omega_n)$. Furthermore, a conjugated equation similar to (49) can be derived for $G_{i0}(t,t')$ and summed,

$$\sum_i t_{0i}(t) G_{i0}(t,t') = \int_C dt_1 \Lambda(t,t_1)\, G(t_1,t')\,, \tag{51}$$

while (49) itself can be rewritten as

$$\int_C dt_1 G^{-1}(t,t_1)\, G_{0j}(t_1,t') = \sum_i t_{0i}(t)\, G^{(0),c}_{ij}(t,t')\,, \quad j \neq 0\,. \tag{52}$$

Summing over (50), these equations can be used to obtain

$$\sum_i t_{0i}(t)\, G_{ij}(t,t') = \int_C dt_1 [G^{-1}(t,t_1) + \Lambda(t,t_1)]\, G_{0j}(t_1,t')\,, \quad j \neq 0\,. \tag{53}$$

Finally, we decompose

$$\begin{aligned} \delta_{0j}\,\delta_C(t,t') &= \sum_l \int_C dt_1 (G^{-1}_{\text{lat}})_{0l}(t,t_1) G_{lj}(t_1,t') \\ &= (i\partial_t + \mu)\, G_{0j}(t,t') - \sum_l t_{0l}(t)\, G_{lj}(t,t') - \int_C dt_1 \sum_l (\Sigma_{\text{lat}})_{0l}(t,t_1)\, G_{lj}(t_1,t')\,, \end{aligned} \tag{54}$$

and use (51) and (53) to arrive at

$$\int_C dt_1 \Sigma(t,t_1) G_{0j}(t_1,t') = \int_C dt_1 \sum_l (\Sigma_{\text{lat}})_{0l}(t,t_1)\, G_{lj}(t_1,t'). \tag{55}$$

Here the cavity site 0 can be replaced by an arbitrary i (for a translationally invariant system),

$$\int_C dt_1 \Sigma(t,t_1)\, G_{ij}(t_1,t') = \int_C dt_1 \sum_l (\Sigma_{\text{lat}})_{il}(t,t_1)\, G_{lj}(t_1,t')\,. \tag{56}$$

Acting on this equation with the inverse of the lattice Green function from the right shows that indeed

$$(\Sigma_{\text{lat}})_{ij}(t,t') = \delta_{ij}\Sigma(t,t') \tag{57}$$

i.e., the lattice self-energy is local in the limit of infinite dimensions and given by the impurity self-energy.

3.4 Self-consistency condition

The DMFT self-consistency condition then corresponds to the Dyson equations for the lattice and impurity Green function. For the lattice Green function it is given by

$$\int_C dt_1 \sum_l \Big[[\delta_{il}\,(i\partial_t + \mu) - t_{il}(t)]\,\delta_C(t,t_1) - \Sigma(t,t_1)\Big]\, G_{lj}(t_1,t') = \delta_{ij}\,\delta_C(t,t')\,, \tag{58}$$

while for the impurity Green function,

$$\int_C dt_1 \,\Big[(i\partial_t + \mu)\,\delta_C(t,t_1) - \Lambda(t,t_1) - \Sigma(t,t_1)\Big]\, G(t_1,t') = \delta_C(t,t')\,. \tag{59}$$

Suppose G has been obtained for given Λ. Then in principle a new Σ can be found from (59) and a new G follows from (58), and then again a new Λ from (59). For the actual strategies regarding the nontrivial numerical solution of the Dyson equations (including Fourier transformation to momentum space) we refer to Refs. [9, 33, 65] as well as [55] and references therein.

3.5 Bethe lattice

As in equilibrium, (44) can directly be evaluated for nearest-neighbor hopping on a Bethe lattice with $\mathcal{Z} \to \infty$ nearest neighbors, $t_{ij} = v/\sqrt{\mathcal{Z}}$, and semielliptic density of states,

$$\rho(\varepsilon) = \frac{\sqrt{4v^2 - \varepsilon^2}}{2\pi v^2}. \tag{60}$$

For neighboring sites i, j of the cavity site 0, $G^{(0),c}_{ij}(t,t')$ is nonzero only for $i = j$, since there is no path from i to j other than through the removed cavity site 0. Furthermore, for $\mathcal{Z} \to \infty$ we have $G^{(0),c}_{i\sigma}(t,t') = G_\sigma(t,t')$. The quantum scaling ensures that the summation over all nearest neighbors of 0 stays finite. This yields the action (43) with the hybridization [66, 24],

$$\Lambda_\sigma(t,t') = v(t)\, G_\sigma(t,t')\, v(t')\,, \tag{61}$$

i.e., after obtaining a new G from S for given hybridization Λ, the new Λ can be obtained at once. The self-energy is nevertheless needed to calculate lattice quantities (such as the lattice Green function or momentum distribution).

3.6 Numerical methods

Several methods have been developed to calculate the contour Green function $G(t,t')$ from the single-site DMFT action (43) for given hybridization $\Lambda(t,t')$ [55]. Generally speaking, these methods are more involved as contour functions on the different branches must be obtained, and not only the initial many-body state (3) must be represented but also its time evolution during which small errors may grow substantially. The methods in the following list all have parameter regimes for which they are well-controlled and therefore accurate, and checking them against each other provides an important benchmark.

Many-body perturbation theory

Diagrammatic perturbation theory [62] is limited to either sufficiently small or large interaction. For weak coupling the self-energy is expanded in terms of Feynman diagrams to a certain finite order in U; see, e.g., Refs. [11, 67, 21, 34, 68, 38, 44, 36, 46]. The Green function lines can be taken as bare or interacting Green functions (as in the equilibrium case [2]), although it is not *a priori* clear which choice is more accurate for a given problem. Strong-coupling perturbation theory is based on a representation in terms of auxiliary particles or an expansion in the hybridization [21, 55]; see, e.g., Refs. [33, 40, 45, 41, 50, 48, 47, 49]. For both small and strong coupling the perturbation expansions are asymptotic in the sense that they will be more accurate if the controlling parameter is smaller. For long times, however, it is never *a priori* clear up to which time they will remain accurate.

Continuous-time quantum Monte Carlo (CT-QMC)

CT-QMC [69–71] also comes in two versions, an interaction and hybridization expansion. Feynman diagrams are generated and sampled stochastically with appropriate weights. In addition to the fermionic sign problem, the imaginary exponents that appear in the contour Green function lead to a dynamic sign problem, so that only comparatively short times can be studied reliably (see, Refs. [20, 21] and Sec. 4). Also, for finite temperatures, an initial thermal state becomes more costly to obtain at low temperatures.

Hamiltonian-based methods

A single-impurity Anderson model (SIAM) with time-dependent couplings and bath energies yields the same nonequilibrium action as (43) with a specific hybridization $\Lambda(t,t')$ upon integrating out the bath. In order to use such a time-dependent SIAM representation this hybridization function must be matched with that obtained from the DMFT self-consistency condition (e.g. (61)), as discussed in detail in [26]. Then, the time evolution of the SIAM Hamiltonian may be obtained by exact diagonalization methods. In general, the accessible time is limited because many bath sites are needed to represent both the correlations in the initial state (which typically decrease with time) and the build-up of correlations in the time-evolved state [26].

Falicov-Kimball model

In the Falicov-Kimball model [72], only one electron species hops between lattice sites while the other is immobile. As in the equilibrium case, it has played an important role for the development of nonequilibrium DMFT [9–11, 13, 15, 18, 19, 29] because it reduces to a quadratic action that is partially solvable. However, its nonequilibrium (and equilibrium) properties are quite different from that of the Hubbard model.

4 Correlated electrons in nonequilibrium

As mentioned in Sec. 1, many aspects of correlated electrons in nonequilibrium have been studied with DMFT. Here we discuss only one of the simplest situations, namely an abrupt change in the Hubbard interaction U.

4.1 Relaxation and thermalization

The evolution of a quantum many-body system in real time raises interesting questions about the connection to equilibrium statistical mechanics. Suppose that an isolated system undergoes some experimental protocol with a Hamiltonian $H(t)$ that no longer changes after a certain time t_1. How does the system behave at large times (during which $H(t \geq t_1) = \text{const}$)? Does it relax to the equilibrium state that is predicted by statistical mechanics for this Hamiltonian $H(t_1)$ for the average energy $E = \text{Tr}[\rho(t_1)H(t_1)]$? If it does, the system is said to *thermalize*. However, the density matrix $\rho(t)$ in (4), when regarded in the eigenbasis of $H(t_1)$, will contain many oscillating components that by themselves will in general not converge. Rather, expectation values (such as Green functions or other short-range correlation functions) will relax to stationary values because they average over many states and degrees of freedom.

In general, the coupling of the system to an environment is needed to prepare a mixed state such as the canonical or grand-canonical Gibbs ensemble (3). This is used in the usual derivation of the Gibbs state in statistical mechanics, based on Boltzmann's concept of entropy $S = k_B \ln \Omega$. The system is coupled to a much larger external thermostat, and the number of available states for the system at energy E is then proportional to the number Ω of microstates of the thermostat at energy $\mathcal{E} - E$, where $\mathcal{E}$ is the fixed total energy of system plus thermostat. Expanding Ω in the vicinity of $\mathcal{E}$ one finds that the probability for the system to have energy E is proportional to $e^{-E/(k_B T)}$, where $T = \partial S/\partial \mathcal{E}$ is the temperature of the thermostat.

On the other hand, during the time evolution of an isolated system there is no environment to assist with the thermalization, i.e., the system must in some sense act as its own environment. *A priori* it is not obvious how the details of the initial state (or $\rho(t_1)$ in the above example) should be irrelevant in the long-time limit so that only a dependence on the average energy remains. The so-called eigenstate thermalization hypothesis [73–76] proposes that this is due to the fact that the expectation value of an observable A in an energy eigenstates with energy E_n usually depends only on the eigenenergy E_n and not on the details of the eigenstate $|n\rangle$. This property can be observed for many generic many-body systems and short-range observables A,

although it is difficult to give precise criteria for its validity. From this property it follows at once that, after relaxation, thermal expectation values are attained for such observables. Integrable systems, on the other hand, are characterized by a large number of conserved quantities. These lead to a dependence of expectation values not only on E_n but also on the individual eigenstates $|n\rangle$. As a consequence, integrable systems usually do not thermalize, a behavior that has also been observed experimentally with cold atoms [77]. Nevertheless, a statistical prediction can often be made using generalized Gibbs ensembles (GGEs), which take the conserved constants of motion (in addition to the Hamiltonian) into account [78, 79, 75]; for reviews see [76, 80]. In general, however, there is still much debate how to even define thermalization or integrability properly for quantum many-body systems in general.

4.2 Interaction quench in the Hubbard model

One of the simplest situations that can be studied in this context is a so-called *quench*, i,e., a sudden switch of Hamiltonians. Here the quench is performed in the Hubbard model (1) at half-filling in the paramagnetic phase with semielliptic density of states (60) with bandwidth $4v \equiv 4$. The system is prepared in the zero-temperature ground state of the noninteracting Hamiltonian, i.e., $U(t < 0) = 0$. At $t = 0$ the Hubbard interaction is switched to a finite value, $U(t \geq 0) = U$. The Green function is obtained with CT-QMC (weak-coupling expansion) from the action (43), and the selfconsistency condition (61) applies [20,21]. The noninteracting initial state makes things simpler because the imaginary branch of the contour does not enter the CT-QMC calculation.

In Fig. 2 the momentum distribution $n(\varepsilon_{\boldsymbol{k}}, t) = \langle c^\dagger_{\boldsymbol{k}\sigma}(t) c_{\boldsymbol{k}\sigma}\rangle$ is plotted as a function of the band energy $\varepsilon \equiv \varepsilon_{\boldsymbol{k}}$ for different final values of U. The the initial Fermi sea evolves from a step function into a continuous function of ε. Fig. 3 shows the jump in the momentum distribution at the Fermi surface and the double occupation as a function of time. Three different parameter regimes can be observed: small and large values of U, separated by a sharp crossover or transition near the intermediate scale $U \approx 3.2 = U_c^{\text{dyn}}$. Near U_c^{dyn}, the momentum distribution relaxes quickly to the thermal distribution for all energies ε (solid blue line in Fig. 2b, obtained from a grand-canonical DMFT equilibrium calculation for the temperature that gives the same total energy E). Relaxation to thermal values is also found for dynamical observables like the retarded Green function $G^R(t+s, t)$ (as a function of time difference s) and the two-time optical conductivity $\sigma(t, t + s)$ [21]. For quenches close to U_c, the system hence thermalizes on short timescales.

For quenches to small or large values of U (away from U_c), thermalization is nevertheless expected on general grounds but cannot be observed on the short time scales that are available with CT-QMC. Away from U_c, the relaxation does not reach a thermal state quickly but instead passes through metastable states on intermediate time scales. For quenches to weak coupling, $U \leq 3$, the double occupation $d(t)$ relaxes from its initial uncorrelated value $d(0) = 1/4$ almost to its thermal value d_{th}, whereas the Fermi surface discontinuity $\Delta n(t)$ remains finite for $t \leq 5$. This behavior is called *prethermalization* and was predicted for a quenched

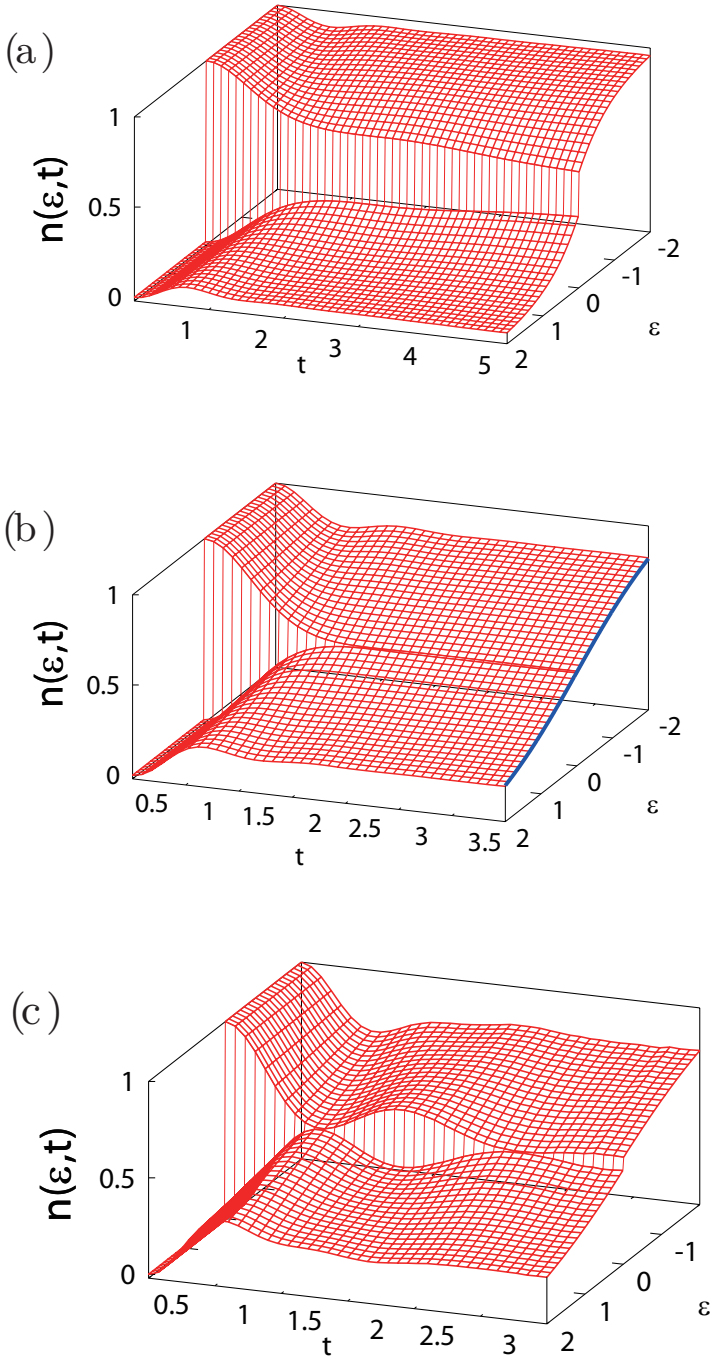

Fig. 2: *Momentum distribution $n(\varepsilon, t)$ after an interaction quench in the Hubbard model with bandwidth 4 in DMFT [20, 21], starting from the noninteracting ground state ($U = 0$) to interaction (a) $U = 2$, (b) $U = 3.3$, (c) $U = 5$. The blue line in (b) is the equilibrium expectation value for the momentum distribution at the same total energy (temperature $T = 0.84$) as the time-evolved state.*

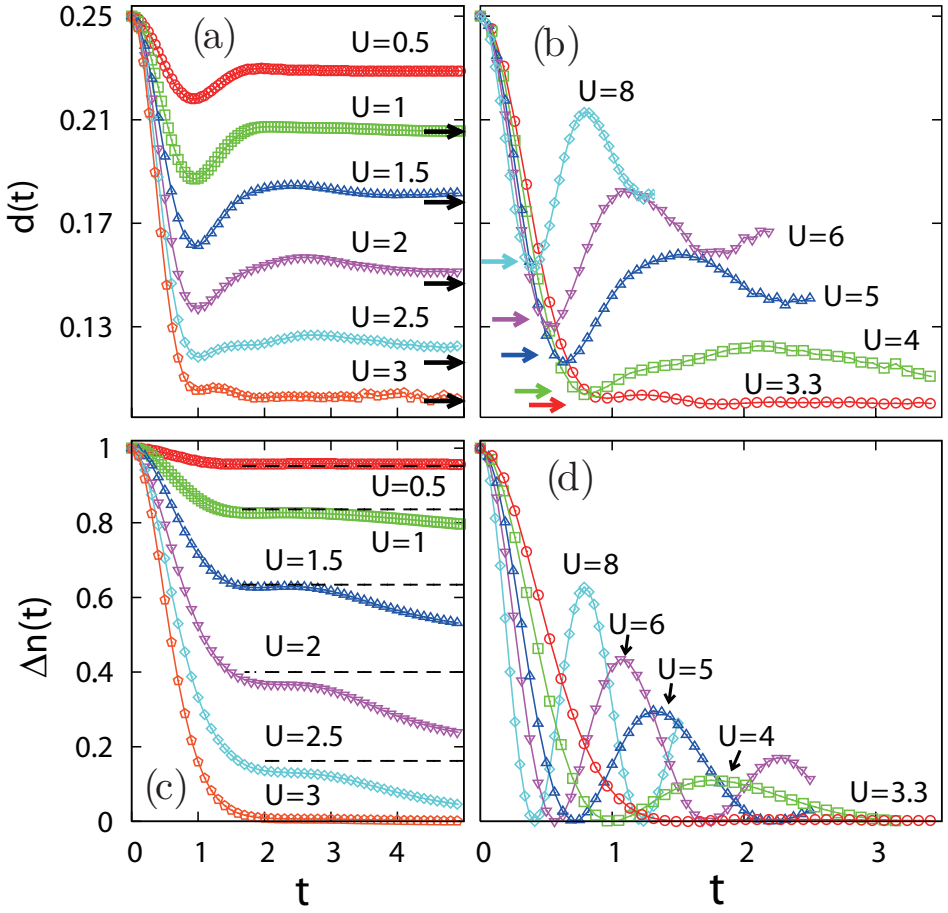

Fig. 3: *Double occupation $d(t)$ and Fermi surface discontinuity Δn after interaction quenches to $U \leq 3$ (left panels) and $U \geq 3.5$ (right panels) [20]. Horizontal arrows: thermal values of the double occupation. Horizontal dashed lines in the lower left panel are the expected prethermalization plateaus [81].*

Fermi liquid [81] on the basis of a weak-coupling calculation. Characteristically, the kinetic and interaction energy thermalize on time scales $1/U^2$ while the Fermi surface discontinuity only reaches a plateau that is located $\Delta n_{\rm stat} = 1 - 2Z$, where Z is the quasiparticle weight in equilibrium at zero temperature. During this early phase the quasiparticles are formed, and during their subsequent scattering the momentum occupations are further redistributed. The weak-coupling result for the transient [81] towards the prethermalization plateau describes the DMFT data well for $U \lesssim 1.5$ [20], even though at the larger U values the timescales $1/U^2$ and $1/U^4$ are no longer well separated. A weakly interacting system may be regarded as nearly integrable, and indeed prethermalization plateaus after an interaction quench are quite generally predicted correctly by a generalized Gibbs ensemble that is built from approximate constants of motion [82]. Physically, the subsequent crossover from the prethermalization plateau to the thermal state is expected due to the scattering of quasiparticles, which can be described by a kinetic equation [83]. Note also that a short-time prethermalization regime has been observed for interaction quenches in the one- and two-dimensional Hubbard model [84, 85, 52], albeit with a less pronounced plateau in the momentum distribution.

For quenches to strong coupling ($U \geq 3.3$ in Fig. 3b,d), the relaxation shows so-called 'collapse-and-revival' oscillations with the approximate periodicity $2\pi/U$, which are due to the exact periodicity of the propagator e^{-iHt} without hopping [6]. For large values of U, both $d(t)$ and $n(\varepsilon, t)$ oscillate around nonthermal values. Strong-coupling perturbation theory [20] shows that the mean value of $d(t)$ for these oscillations is $d_{\text{stat}} = d(0) - \Delta d$ with $\Delta d = (1/2U)\langle H_{\text{kin}}/L\rangle_{t=0}$. By contrast, the thermal value is obtained as $d_{\text{th}} = d(0) + (1/U)\langle H_{\text{kin}}/L\rangle_0$ from a high-temperature expansion. Hence, during the initial stage of the relaxation the double occupation relaxes only halfway towards d_{th}. Although longer times cannot be accessed with the weak-coupling CT-QMC method, a relaxation to the thermal state is expected after the oscillations have decayed, as in the case of a pump-excited Mott insulator [33]. In general, this crossover will set in only on times scales that are exponentially large in the interaction U [86].

The rapid thermalization at $U \approx U_c^{\text{dyn}}$ occurs at the border between the delayed thermalization either due to weak-coupling prethermalization plateaus or strong-coupling oscillations around nonthermal values. Indeed, no finite width was detected for the width of this crossover region, so that the behavior at U_c^{dyn} might signal a dynamical phase transition. A similarly strong dependence on the quenched interaction was observed in Heisenberg chains [87] and the one-dimensional Hubbard model [84]. Several possible origins for nonequilibrium phase transitions of this type have been proposed [88–91]. For the DMFT data, the corresponding equilibrium temperature T_{eff} after the quench is much higher than the critical endpoint of the Mott metal-insulator transition in equilibrium ($T_c \approx 0.055$ [2], but $T_{\text{eff}} = 0.84$ for $U = 3.3$). Interestingly, a good approximation for the critical interaction, $U_c^{\text{dyn}} \approx 3.4$, is obtained from a time-dependent variational theory using the Gutzwiller approximation [92, 93]. Variational results also suggest that the difference in U_c for equilibrium and nonequilibrium is due to the rapid change in interaction and corresponding high excitation energy: if the Hubbard interaction is instead changed very slowly, this lessens the effective temperature and the dynamical critical value U_c approaches that of the equilibrium transition [94].

Acknowledgment

Support of the Deutsche Forschungsgemeinschaft through FOR1346 is gratefully acknowledged.

References

[1] W. Metzner and D. Vollhardt, Phys. Rev. Lett. **62**, 324 (1989)

[2] A. Georges, G. Kotliar, W. Krauth, and M.J. Rozenberg, Rev. Mod. Phys. **68**, 13 (1996)

[3] A.L. Cavalieri, N. Müller, T. Uphues, V.S. Yakovlev, A. Baltuška, B. Horvath, B. Schmidt, L. Blümel, R. Holzwarth, S. Hendel, M. Drescher, U. Kleineberg, P.M. Echenique, R. Kienberger, F. Krausz, and U. Heinzmann, Nature **449**, 1029 (2007)

[4] S. Wall, D. Brida, S.R. Clark, H.P. Ehrke, D. Jaksch, A. Ardavan, S. Bonora, H. Uemura, Y. Takahashi, T. Hasegawa, H. Okamoto, G. Cerullo, and A. Cavalleri, Nature Phys. **7**, 114 (2011)

[5] R. Peierls, Z. Physik **80**, 763 (1933)

[6] M. Greiner, O. Mandel, T.W. Hänsch, and I. Bloch, Nature **419**, 51 (2002)

[7] I. Bloch, J. Dalibard, and W. Zwerger, Rev. Mod. Phys. **80**, 885 (2008)

[8] V. Turkowski and J.K. Freericks, Phys. Rev. B **71**, 085104 (2005)

[9] J.K. Freericks, V.M. Turkowski, and V. Zlatić, Phys. Rev. Lett. **97**, 266408 (2006)

[10] J.K. Freericks, Phys. Rev. B **77**, 075109 (2008)

[11] V. Turkowski and J.K. Freericks, Phys. Rev. B **75**, 125110 (2007)

[12] V. Turkowski and J.K. Freericks, Phys. Rev. B **77**, 205102 (2008); Erratum: *ibid.* **82**, 119904 (2010)

[13] M.-T. Tran, Phys. Rev. B **78**, 125103 (2008)

[14] A.V. Joura, J.K. Freericks, and T. Pruschke, Phys. Rev. Lett. **101**, 196401 (2008)

[15] M. Eckstein and M. Kollar, Phys. Rev. Lett. **100**, 120404 (2008)

[16] P. Schmidt and H. Monien: *Nonequilibrium dynamical mean-field theory of a strongly correlated system*. Preprint arXiv:cond-mat/0202046

[17] J.K. Freericks, H.R. Krishnamurthy, and T. Pruschke, Phys. Rev. Lett. **102**, 136401 (2009)

[18] M. Eckstein and M. Kollar, Phys. Rev. B **78**, 205119 (2008)

[19] M. Eckstein and M. Kollar, Phys. Rev. B **78**, 245113 (2008)

[20] M. Eckstein, M. Kollar, and P. Werner, Phys. Rev. Lett. **103**, 056403 (2009)

[21] M. Eckstein, M. Kollar, and P. Werner, Phys. Rev. B **81**, 115131 (2010)

[22] M. Eckstein and P. Werner, Phys. Rev. B **82**, 115115 (2010)

[23] P. Werner and M. Eckstein, Phys. Rev. B **86**, 045119 (2012)

[24] M. Eckstein and M. Kollar, New J. Phys. **12**, 055012 (2010)

[25] N. Eurich, M. Eckstein, and P. Werner, Phys. Rev. B **83**, 155122 (2011)

[26] C. Gramsch, K. Balzer, M. Eckstein, and M. Kollar, Phys. Rev. B **88**, 235106 (2013)

[27] A. Lubatsch and J. Kroha, Ann. Phys. **18**, 863 (2009)

[28] N. Tsuji, T. Oka, and H. Aoki, Phys. Rev. B **78**, 235124 (2008)

[29] N. Tsuji, T. Oka, and H. Aoki, Phys. Rev. Lett. **103**, 047403 (2009)

[30] B. Moritz, T.P. Devereaux, and J.K. Freericks, Phys. Rev. B **81**, 165112 (2010)

[31] B. Moritz, A.F. Kemper, M. Sentef, T.P. Devereaux, and J.K. Freericks, Phys. Rev. Lett. **111**, 077401 (2013)

[32] M. Eckstein, T. Oka, and P. Werner, Phys. Rev. Lett. **105**, 146404 (2010)

[33] M. Eckstein and P. Werner, Phys. Rev. B **84**, 035122 (2011)

[34] M. Eckstein and P. Werner, Phys. Rev. Lett. **107**, 186406 (2011)

[35] N. Tsuji, T. Oka, P. Werner, and H. Aoki, Phys. Rev. Lett. **106**, 236401 (2011)

[36] N. Tsuji, T. Oka, H. Aoki, and P. Werner, Phys. Rev. B **85**, 155124 (2012)

[37] K. Mikelsons, J.K. Freericks, and H.R. Krishnamurthy, Phys. Rev. Lett. **109**, 260402 (2012)

[38] A. Amaricci, C. Weber, M. Capone, and G. Kotliar, Phys. Rev. B **86**, 085110 (2012)

[39] C. Aron, Phys. Rev. B **86**, 085127 (2012)

[40] M. Eckstein and P. Werner, Phys. Rev. Lett. **110**, 126401 (2013)

[41] M. Eckstein and P. Werner, J. Phys.: Conf. Series **427**, 012005 (2012)

[42] C. Aron, C. Weber, and G. Kotliar, Phys. Rev. B **87**, 125113 (2013)

[43] J. Mentink and M. Eckstein: *Ultrafast quenching of the exchange interaction in a Mott insulator*. Preprint arXiv:1401.5308

[44] N. Tsuji, M. Eckstein, and P. Werner, Phys. Rev. Lett. **110**, 136404 (2013)

[45] P. Werner, N. Tsuji, and M. Eckstein, Phys. Rev. B **86**, 205101 (2012)

[46] N. Tsuji and P. Werner, Phys. Rev. B **88**, 165115 (2013)

[47] M. Eckstein and P. Werner: *Ultrafast separation of photo-doped carriers in Mott antiferromagnets*. Preprint arXiv:1403.1461

[48] P. Werner and M. Eckstein, Phys. Rev. B **88**, 165108 (2013)

[49] P. Werner and M. Eckstein: *Field-induced polaron formation in the Holstein-Hubbard model*. Preprint arXiv:1403.7376

[50] M. Eckstein and P. Werner, Phys. Rev. B **88**, 075135 (2013)

[51] C. Jung, A. Lieder, S. Brener, H. Hafermann, B. Baxevanis, A. Chudnovskiy, A. Rubtsov, M. Katsnelson, and A. Lichtenstein, Ann. Phys. (Berlin) **524**, 49 (2012)

[52] N. Tsuji, P. Barmettler, H. Aoki, and P. Werner: *Nonequilibrium dynamical cluster theory*. Preprint arXiv:1307.5946

[53] F. Hofmann, M. Eckstein, E. Arrigoni, and M. Potthoff, Phys. Rev. B **88**, 165124 (2013)

[54] H.U.R. Strand, M. Eckstein, and P. Werner: *Nonequilibrium dynamical mean-field theory for bosonic lattice models*. Preprint arXiv:1405.6941

[55] H. Aoki, N. Tsuji, M. Eckstein, M. Kollar, T. Oka, and P. Werner, Rev. Mod. Phys. **86**, 779 (2014)

[56] A.L. Fetter and J.D. Walecka: *Quantum Theory of Many-Particle Systems* (Dover, New York, 2003)

[57] J. Schwinger, J. Math. Phys. **2**, 407 (1961)

[58] L.P. Kadanoff and G. Baym: *Quantum Statistical Mechanics* (W.A. Benjamin, New York, 1962)

[59] L.V. Keldysh, Zh. Eksp. Teor. Fiz. **47**, 1515 (1964) [Sov. Phys. JETP **20**, 1018 (1965)]

[60] A. Kamenev: *Field Theory of Non-Equilibrium Systems* (Cambridge Univ. Press, 2011)

[61] R. van Leeuwen, N.E. Dahlen, G. Stefanucci, C.-O. Almbladh, and U. von Barth: *Introduction to the Keldysh formalism*, Lecture Notes in Physics, Vol. 706 (Spinger, Heidelberg, 2006)

[62] G. Stefanucci and R. van Leeuwen: *Non-Equilibrium Many-Body Theory of Quantum Systems* (Cambridge University Press, 2013)

[63] R. van Leeuwen and G. Stefanucci, J. Phys.: Conf. Series **427**, 012001 (2013)

[64] D.C. Langreth in *Linear and Nonlinear Electron Transport in Solids* ed. by J.T. Devreese and V.E. van Doren (Plenum Press, New York, 1976)

[65] K. Balzer and M. Eckstein, Phys. Rev. B **89**, 035148 (2014)

[66] M. Eckstein, A. Hackl, S. Kehrein, M. Kollar, M. Moeckel, P. Werner, and F.A. Wolf, Eur. Phys. J. Special Topics **180**, 217 (2010)

[67] R.J. Heary and J.E. Han, Phys. Rev. B **80**, 035102 (2009)

[68] C. Aron, G. Kotliar, and C. Weber, Phys. Rev. Lett. **108**, 086401 (2012)

[69] L. Mühlbacher and E. Rabani, Phys. Rev. Lett. **100**, 176403 (2008)

[70] P. Werner, T. Oka, and A.J. Millis, Phys. Rev. B **79**, 035320 (2009)

[71] E. Gull, A.J. Millis, A.I. Lichtenstein, A.N. Rubtsov, M. Troyer, and P. Werner, Rev. Mod. Phys. **83**, 349 (2011)

[72] J.K. Freericks and V. Zlatić, Rev. Mod. Phys. **75**, 1333 (2003)

[73] M. Srednicki, Phys. Rev. E **50**, 888 (1994)

[74] J.M. Deutsch, Phys. Rev. A **43**, 2046 (1991)

[75] M. Rigol, V. Dunjko, and M. Olshanii, Nature **452**, 854 (2008)

[76] A. Polkovnikov, K. Sengupta, A. Silva, and M. Vengalattore, Rev. Mod. Phys. **83**, 863 (2011)

[77] T. Kinoshita, T. Wenger, and D.S. Weiss, Nature **440**, 900 (2006)

[78] E.T. Jaynes, Phys. Rev. **106**, 620 (1957)

[79] E.T. Jaynes, Phys. Rev. **108**, 171 (1957)

[80] J. Dziarmaga, Adv. Phys. **59**, 1063 (2010)

[81] M. Moeckel and S. Kehrein, Phys. Rev. Lett. **100**, 175702 (2008)

[82] M. Kollar, F.A. Wolf, and M. Eckstein, Phys. Rev. B **84**, 054304 (2011)

[83] M. Stark and M. Kollar: *Kinetic description of thermalization dynamics in weakly interacting quantum systems*. Preprint arXiv:1308.1610

[84] S.A. Hamerla and G.S. Uhrig, Phys. Rev. B **87**, 064304 (2013)

[85] S.A. Hamerla and G.S. Uhrig, Phys. Rev. B **89**, 104301 (2014)

[86] R. Sensarma, D. Pekker, E. Altman, E. Demler, N. Strohmaier, D. Greif, R. Jördens, L. Tarruell, H. Moritz, and T. Esslinger, Phys. Rev. B **82**, 224302 (2010)

[87] P. Barmettler, M. Punk, V. Gritsev, E. Demler, and E. Altman, Phys. Rev. Lett. **102**, 130603 (2009)

[88] B. Sciolla and G. Biroli, Phys. Rev. Lett. **105**, 220401 (2010)

[89] A. Gambassi and P. Calabrese, EPL **95**, 66007 (2011)

[90] M. Heyl, A. Polkovnikov, and S. Kehrein, Phys. Rev. Lett. **110**, 135704 (2013)

[91] C. Karrasch and D. Schuricht, Phys. Rev. B **87**, 195104 (2013)

[92] M. Schiró and M. Fabrizio, Phys. Rev. Lett. **105**, 076401 (2010)

[93] M. Schiró and M. Fabrizio, Phys. Rev. B **83**, 165105 (2011)

[94] M. Sandri, M. Schiró, and M. Fabrizio, Phys. Rev. B **86**, 075122 (2012)